Nanoscale

REVIEW

View Article Online
View Journal | View Issue

Cite this: *Nanoscale*, 2014, **6**, 8444

Plasmonic nanostructures for light trapping in organic photovoltaic devices

Chun-Hsien Chou[a] and Fang-Chung Chen*[b]

Received 23rd April 2014
Accepted 19th May 2014

DOI: 10.1039/c4nr02191f

www.rsc.org/nanoscale

Over the past decade, we have witnessed rapid advances in the development of organic photovoltaic devices (OPVs). At present, the highest level of efficiency has surpassed 10%, suggesting that OPVs have great potential to become competitive with other thin-film solar technologies. Because plasmonic nanostructures are likely to further improve the efficiency of OPVs, this Article reviews recent progress in the development of metal nanostructures for triggering plasmonic effects in OPVs. First, we briefly describe the physical fundamentals of surface plasmons (SPs). Then, we discuss recent approaches toward increasing the light trapping efficiency of OPVs through the incorporation of plasmonic structures. Finally, we provide a brief outlook into the future use of SPs in highly efficient OPVs.

1 Introduction

The use of traditional fossil fuels is leading to increasing environmental concerns, including air pollution, global warming, and possibly climatic anomalies. To sustain economic growth, renewable energy sources, such as solar energy and wind power, are being considered as promising energy alternatives. The development of solar energy is a particularly suitable solution to the energy crisis because sunlight is clean, sustainable, and naturally abundant. Nevertheless, wafer-based solar cells, which have the major share of the current photovoltaic market, are not capable of producing energy at a price comparable to that of electricity generated from fossil fuels in most areas of the world.[1] Therefore, the quest remains for inexpensive, scalable, next-generation solar technologies.

Among emerging solar technologies, organic photovoltaics (OPVs) are receiving a great deal of attention because of their attractive properties: low cost, light weight, mechanical flexibility,[2,3] and extremely short energy payback time.[4,5] Recently, the power conversion efficiencies (PCEs) of OPVs prepared using the concept of bulk heterojunctions (BHJs) have approached 10%,[6,7] with the highest recorded efficiency having broken through 10% (ref. 8–12) for a tandem structure. These

[a]*Department of Photonics and Institute of Electro-Optical Engineering, National Chiao Tung University, Hsinchu 30010, Taiwan*
[b]*Department of Photonics and Display Institute, National Chiao Tung University, Hsinchu 30010, Taiwan. E-mail: fcchen@mail.nctu.edu.tw*

Chun-Hsien Chou received his Bachelor's degree from the Department of Physics in Fu Jen Catholic University in 2006 and his Master's degree from the Institute of Physics in National Taiwan Normal University in 2008. Prior to joining National Chiao Tung University (NCTU) in 2011, he worked in the PV industry as a R&D engineer for two years. He is currently a Ph.D. student in the field of organic solar cells and flexible waveguiding photovoltaics in the group of Prof. Chen at NCTU, Taiwan.

Dr Fang-Chung Chen is a professor in the Department of Photonics at National Chiao Tung University (NCTU). He received his Bachelor's and Master's degrees in Chemistry from National Taiwan University in 1996 and 1998, respectively, and his Ph.D. degree in Materials Science and Engineering from the University of California, Los Angeles (UCLA), USA, in 2003. He was a postdoctoral research associate in the Department of Materials Science and Engineering, UCLA, in 2003. Prof. Chen is the recipient of the Award for Junior Research Investigators of Academia Sinica 2008. His research interests include flexible solar cells, organic electronics, and low-dimentsional nanomaterials.

efficiencies remain, however, lower than those of other thin-film solar technologies, such as CdTe and CIGS photovoltaics. In other words, continuous improvements in efficiency will be necessary if OPVs are to become commercially viable. Moreover, the reliability of OPVs must be improved substantially to meet commercial requirements.[13]

The working principle of a typical OPV involves six steps:[14] (i) photon absorption, (ii) exciton generation, (iii) exciton diffusion, (iv) exciton dissociation, (v) charge transport, and (vi) charge collection. Electron/hole pairs (excitons) are generated upon the absorption of photons in organic semiconductors. Because the exciton binding energy is usually large (0.3–1 eV), they can be dissociated into free charges only at the interfaces between strong electron donors and electron acceptors. Therefore, a BHJ structure is often adopted to ensure a large-area donor–acceptor interface, thereby producing a high density of free charge carriers. The free charges at the heterojunctions are then transported through the donor and acceptor materials, respectively, to the electrodes. The collection of the charges by the electrodes results in the generation of electrical power. The efficiencies of the above-mentioned processes are often evaluated in terms of the external quantum efficiency (EQE), also known as the incident photon-to-electron conversion efficiency (IPCE), using the equation,[15]

$$\mathrm{EQE}(\lambda) = \eta_{\mathrm{ab}}(\lambda) \times \eta_{\mathrm{gen}}(\lambda) \times \eta_{\mathrm{coll}}(\mu) \quad (1)$$

where $\eta_{\mathrm{ab}}(\lambda)$, $\eta_{\mathrm{gen}}(\lambda)$, and $\eta_{\mathrm{coll}}(\mu)$ are the efficiencies of absorption, carrier generation, and charge collection, respectively. The efficiency of carrier generation can reach almost 100% in a BHJ solar cell because of its high donor–acceptor interfacial area. It is very difficult, however, to simultaneously improve the efficiencies of absorption and charge collection. While thicker photoactive layers can be used to increase the value of $\eta_{\mathrm{ab}}(\lambda)$, the possibility of charge recombination and the inevitable increase in the device series resistance will result in a lower value of $\eta_{\mathrm{coll}}(\mu)$.[16] Therefore, the tradeoff always exists between a high degree of light absorption and efficient charge collection.

One approach toward ensuring efficient light absorption when using a thin photoactive layer is to develop light trapping schemes. Many trapping strategies for OPVs have been proposed, including using optical spacers,[17–20] photonic crystals,[21,22] and folded device architectures.[23] More recently, metal nanostructures, which trigger surface plasmons (SPs), have proved to be promising materials for effective light trapping in thin-film solar cells.[24–27] Surface plasmons are coherent oscillations of electromagnetic waves propagating along the surface of a conductor. They were first discovered by Faraday during his study of the colors of colloidal metal nanoparticles (NPs).[28] Several particle shapes (*e.g.*, spheres, prisms, cubes, rice grains, stars)[29–37] and periodic structures on the nanoscale (*e.g.*, metal nanohole,[38,39] nanodiscs,[29,40] nanopillars[41,42] and nanogratings[43,44] arrays) have been successfully developed to induce SPs, with the optical properties readily tailored through modifications in their sizes, shapes, and even the surrounding dielectric materials.[45] Accordingly, these nanostructures have great potential as effective optical tools for enhancing the absorption properties of OPVs.

In this Review Article, we first introduce the concept of SPs. We then focus on the results of recent research into the development of potential plasmonic-enhanced OPVs. Finally, we provide a short summary and perspective regarding the future use of plasmonic nanostructures in highly efficient OPVs.

2 Physical properties of surface plasmons

2.1. Localized surface plasmons

Localized surface plasmons (LSPs) are associated with the collective oscillations of electrons confined locally by metal nanostructures. As displayed in Fig. 1(a), the most representative examples of LSPs are metal NPs. The particle plasmons are excited when the frequency of the incident photons matches the resonance frequency of the NPs. Their resonance wavelength depends on the particle shape, size, and the dielectric parameters of the surrounding environment.[32,46,47] From the quasi-static approximation, the polarizability (P) of a spherical NP can be expressed as:

$$P = 4\pi a^3 \frac{\varepsilon - \varepsilon_{\mathrm{m}}}{\varepsilon + 2\varepsilon_{\mathrm{m}}} \quad (2)$$

where a is the diameter of the NP and ε and ε_{m} are the dielectric constants of the surrounding dielectric medium and of the metal NP itself, respectively. From eqn (2), we conclude that the value of P reaches its maximum when ε_{m} is equal to -2ε, resulting in a resonance condition. Because the excited plasmons are localized and cannot propagate within the nanostructure, this process is known as localized surface plasmon resonance (LSPR).

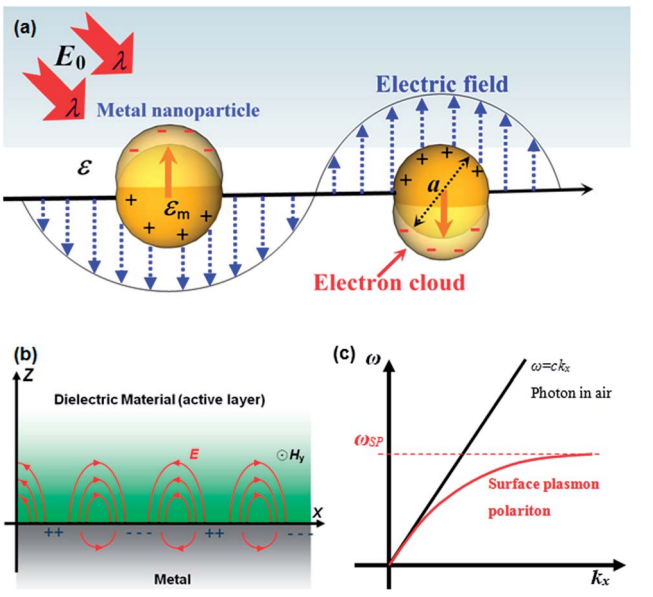

Fig. 1 (a) LSPs confined in metal NPs. The SPs are excited by the electric field (E_0) of the incident light of wavelength λ in spherical NPs of diameter a. (b) Schematic representation of the SPP mode excited at the metal–dielectric interface.[49] (c) Dispersion curve of a typical SPP mode; a momentum mismatch exists between the light and the SPP.[49]

If we assume that the size of the NP is much smaller than the incident wavelength ($a \ll \lambda$), then the cross-sections of light scattering (σ_{sca}) and absorption (σ_{ab}) are given by:[26,48]

$$\sigma_{sca} = \frac{1}{6\pi}\left(\frac{2\pi}{\lambda}\right)^4 |P|^2 = \frac{8\pi}{3}k^4a^6\left|\frac{\varepsilon - \varepsilon_m}{\varepsilon + 2\varepsilon_m}\right|$$
$$\sigma_{ab} = \frac{2\pi}{\lambda}\mathrm{Im}[P] = 4\pi k a^3 \frac{\varepsilon - \varepsilon_m}{\varepsilon + 2\varepsilon_m} \quad (3)$$

where k is the wavenumber of the light. Further, the scattering efficiency (Q_{sc}) can be defined as:[26]

$$Q_{sc} = \sigma_{sca}/(\sigma_{sca} + \sigma_{ab}) \quad (4)$$

According to eqn (3), the particle size is entirely responsible for the extinction process;[25,46] larger particles scatter light more efficiently, whereas smaller ones absorb most of the photons. One unique feature of LSPs is the local enhancement of the electromagnetic field as a result of the strong resonance effects, leading to effective light concentration. The enhancement factor can reach as high as 100.[50] Such a plasmonic near field in the vicinity of an NP decays exponentially with respect to the distance from the surface of the NP. The decay lengths of the electrical field are usually of the order of the particle size, but also depend on the dielectric properties of the surroundings and the metallic material itself.[24,32,46]

2.2. Surface plasmon polaritons

The other types of excited SPs on metal surfaces are surface plasmon polaritons (SPPs), collective oscillations of electromagnetic waves at a metal–dielectric interface [Fig. 1(b)]. The electromagnetic field of an SPP is confined at the metal surface, with the electric field also enhanced perpendicular to the surface. From Maxwell's equations, the dispersion relationship for a typical SPP can be derived using the equation:[48]

$$K_{sp} = \frac{\omega}{c}\sqrt{\frac{\varepsilon_d\varepsilon_m}{\varepsilon_d + \varepsilon_m}} \quad (5)$$

where K_{sp} is the wave vector of the SPP; ε_d and ε_m are the relative permittivities of the dielectric and metal materials, respectively; and ω and c are the angular frequency and the speed of light in a vacuum, respectively. Fig. 1(c) displays the dispersion curve of an SP mode; a momentum mismatch exists between the photon and the SPP, implying that direct excitation of SPPs with photons is not allowed in the case of a planar interface. Three approaches have been developed to match their momenta:[24,49] (i) to use a prism covered with a thin layer of metal to increase the momentum of the incident light; (ii) to apply scattering centers to trigger SPs; and (iii) to employ periodic corrugated structures, such as gratings, at the interface. The third is the most common approach used in OPVs, presumably because of compatibility with thin-film devices. In the next section, we discuss several examples of periodic nanostructures that have successfully improved the performance of OPVs.

2.3. Device structures for plasmonic-enhanced OPVs

Three common device structures have been developed employing plasmonic nanostructures to enhance the OPV performance (Fig. 2).[24–26] The first design involves the incorporation of metal nanostructures, such as NPs, on the surface of the active organic layers; they behave as scattering centers that can trap the light in the device. The optical path will be increased through multiple scattering events, thereby increasing the photon absorption efficiency. In the second scenario, NPs are directly embedded into the active photoactive layer. Relatively small NPs (5–20 nm) will act as subwavelength antennas upon photoexcitation, thereby inducing the local-field enhancement. Because the absorption efficiency of the organic layers is proportional to the intensity of the electromagnetic field, the overall device efficiency can be improved. Nevertheless, such an ideal structure as displayed in Fig. 2(b) is very difficult to realize because the NPs will phase-separate from the organic semiconductors, thereby increasing the device resistance. Therefore, the nanostructures should be carefully designed to control the distribution of the NPs in the photoactive layers.[25,51] In the final case, as depicted in Fig. 2(c), periodic corrugated nanostructures are included at the interface between the metal electrode and the absorption layer to sustain propagating SPPs. The evanescent electromagnetic fields excited by the incident light effectively direct the vertical energy into the semiconductor layer. Such a design ensures that photons are absorbed along the lateral direction and that the optical path is increased by several orders of magnitude with respect to the thickness of the active layer. In other words, high absorption efficiency can theoretically be achieved from a thin film.

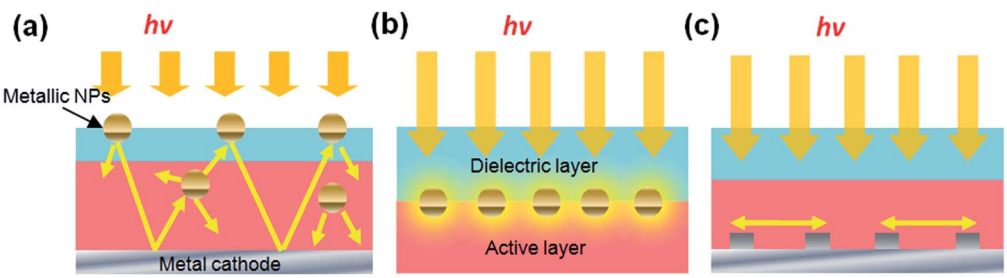

Fig. 2 Structure designs of plasmonic-enhanced OPVs.[24,25,48] (a) Nanostructures behaving as scattering centers; incident photons are scattered mostly into the material having a higher dielectric constant at the thin film surface. (b) Embedded NPs positioned in organic semiconductors to enhance the near-field in the cell; scattering events also possibly occur in such solar cells. (c) A periodical structure induces SPPs, which can turn the incident solar flux by 90°.

3 Experimental results of plasmonic OPVs

3.1 NPs positioned in the vicinity of the photoactive layer

3.1.1 Spherical NPs. The use of metal NPs is the most common means of obtaining plasmonic-enhanced OPVs because of the simplicity of their fabrication.[26,46,52–54] In 2008, for example, Morfa *et al.* deposited Ag NPs through thermal evaporation on indium tin oxide (ITO) substrates[55] and then spin-coated a layer of poly(3,4-ethylenedioxythiophene):polystyrenesulfonate (PEDOT:PSS) buffer onto the NPs. When using a blend of poly-(3-hexylthiophene) (P3HT) and [6,6]-phenyl-C_{61}-butyric acid methyl ester ($PC_{60}BM$) as the photoactive layer, the device PCE increased from 1.3 to 2.2% after the incorporation of the Ag NPs. Other methods, such as pulse-current electrode deposition, have been also used for the synthesis of the noble metallic NPs.[56,57] Kim *et al.* demonstrated that a relatively uniform distribution of NPs could be achieved through such electrochemical deposition; their device PCE increased from 3.05 to 3.69% after introduction of the Ag NPs.[58]

Another noble metal, gold, can also produce LSPR phenomena. In 2009, we blended Au NPs into the anodic buffer layer (PEDOT:PSS) of OPVs to trigger LSPR.[54,59] Because NP solutions are frequently prepared in water through colloidal chemistry,[60,61] buffer solutions containing Au NPs are readily prepared through blending of Au NP and PEDOT:PSS solutions [Fig. 3(a)]. This relatively simple plasmon-enhancing layer improved the device PCE from 3.57 to 4.24%. Another benefit of such a simple fabrication approach is highly repeatable results, allowing systematic studies of the mechanism behind the enhancement in PCE. Fig. 3(b) presents the increase in quantum efficiencies after incorporating Au NPs, compared with the extinction spectrum of the Au NPs. The difference in the incident photon–electron conversion efficiency (ΔIPCE) spectrum coincides with the extinction range of the Au NPs, indicating that the LSPR did indeed improve the photocurrent.

To further investigate the near-field effect, steady-state photoluminescent (PL) spectra of the P3HT:PCBM films were obtained; the sample deposited on the PEDOT:PSS layer doped with Au NPs exhibited higher intensity, suggesting an increased level of photoabsorption.[48] We also performed exciton lifetime mapping of the photoabsorbing film by using a time-resolved PL measurement system together with confocal laser scanning microscopy, which allowed vertical evolution of the exciton lifetime ($\tau_{exciton}$) in the thin films at various *z*-axial positions.[62] Fig. 3(c–f) display histograms of the vertical evolutions of $\tau_{exciton}$ in thin films prepared under various conditions. For the reference sample, the average value of $\tau_{exciton}$ was 0.48 ns when the focal plane was close to the PEDOT:PSS layer. The lifetime decreased to 0.35 ns when the focal plane was positioned away from the PEDOT:PSS buffer. The inhomogeneous distribution of the $PC_{60}BM$ molecules in the P3HT could account for the lifetime evolution.[62] Completely opposite behavior was observed for the samples containing Au NPs in the PEDOT:PSS layers. The value of $\tau_{exciton}$ decreased to 0.23 ns, presumably because of strong coupling between the plasmons and excitons.

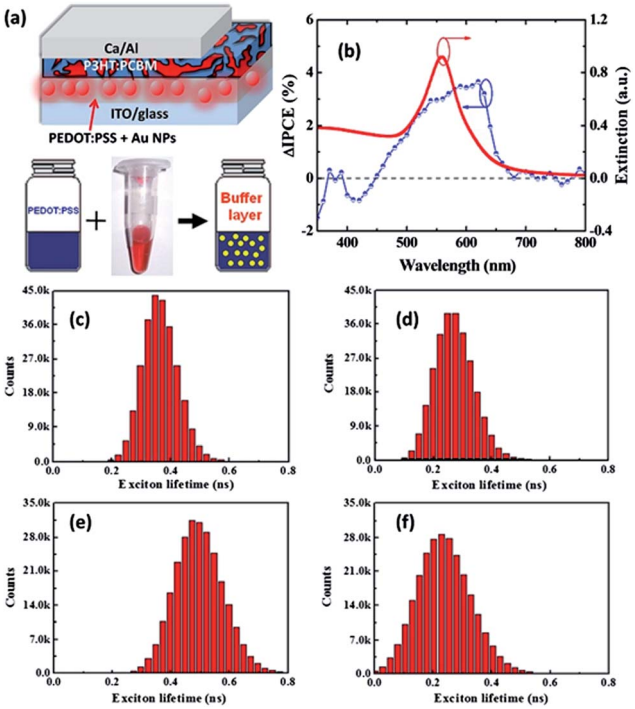

Fig. 3 (a) Device structure of OPV containing Au NPs and the method of preparation of the buffer solution containing Au NPs.[59] (b) The change in IPCE after blending the Au NPs, compared with the extinction spectrum of the Au NPs. (c–f) Histograms of the exciton lifetimes for the (c and e) reference and (d and f) plasmonic devices at the positions (c and d) away from and (e and f) close to the PEDOT:PSS buffer layer. Average values of $\tau_{exciton}$: (c) 0.35, (d) 0.27, (e) 0.48, and (f) 0.23 ns.[54]

Furthermore, the values of $\tau_{exciton}$ of the upper positions, away from the surfaces of the metal NPs, were less affected, suggesting that near-field plasmonic effects contributed significantly to the device enhancement.

Although PEDOT:PSS is the material most widely used for the anode buffers, its acidity and hygroscopic properties usually result in poor device stability.[63] Therefore, several alterative buffer materials have been tested to improve the reliability of plasmonic-enhanced OPVs. For example, solution-processed molybdenum oxides (MoO_3)[64] have been blended with Au NPs; the mixed solutions were then spin-coated onto ITO substrates, with the resulting nanocomposite layer becoming an anode buffer for OPVs.[64,65] The device exhibited a remarkable enhancement in PCE after the incorporation of Au NPs. Moreover, the stability of devices prepared using a MoO_3 buffer is superior to that of devices based on PEDOT:PSS buffers.[64] Furthermore, because inverted device architectures eliminate the need for low-work function metals, which are air-sensitive,[63] they usually exhibit prolonged device lifetimes.[66,67] The upper polymer layers also naturally behave as protective shields from oxygen and moisture in the air. Plasmonic-enhanced OPVs possessing an inverted device structure have also been demonstrated.[68–70] A mixed solution of Au NP/Cs_2CO_3 was applied in inverted OPVs having the structure ITO/Au NP:Cs_2CO_3/P3HT:PCBM/MoO_3/Ag. The photocurrents and fill

factors both improved after the addition of Au NPs to the Cs_2CO_3 buffer layer; overall, the PCE increased from 3.12 to 3.54%. A study of the morphologies of the cathode interfaces revealed that rough surfaces might increase the device resistance; this drawback is, however, overshadowed by the advantageous plasmonic effects.[68]

Aggregation of NPs in PEDOT:PSS is often observed unless a capping agent is applied.[71] To overcome this issue and to further control the uniformity of the NP distribution, Fan *et al.* used graphene oxide (GO) as the template to construct metal nanostructures to trigger SPs in OPVs.[71] Au NPs were first adhered to the GO surface and then blended into the PEDOT:PSS layer. The GO template helped to avoid aggregation of the Au NPs and to introduce plasmonic effects without dramatically sacrificing the device's electrical properties.[71] Moreover, GO itself and its reduced form (rGO) are effective interlayers when positioned between the electrodes and the photoactive layer in OPVs.[72,73] We recently reported the synthesis and characterization of Au NP/GO nanocomposites for the triggering of LSPRs.[74] The morphology of the Au NPs on the GO surface was manipulated by controlling the amount of capping agent during the synthesis steps. When the nanomaterials served as the anodic interlayer, they introduced LSPR effects in the OPVs, leading to a noticeable enhancement in efficiency. That study implies new avenues for constructing plasmon-enhancing layers on the nanoscale.

In addition to blending with P3HT:PCBM, the most well-known model polymer mixture, to construct BHJ solar cells, the metal NPs have been also applied in other material systems. In principle, the open-circuit voltage (V_{oc}) is highly related to the energy difference between the highest occupied molecular orbital (HOMO) of the polymer semiconductor and the lowest unoccupied molecular orbital (LUMO) of the fullerene derivative.[75,76] In other words, if $PC_{60}BM$ is replaced by another electron acceptor and the value of V_{oc} is increased, the overall PCE will be improved. The representative acceptor was indene-C_{60} bisadduct (ICBA); its LUMO, higher than that of $PC_{60}BM$, has been proved to increase the photovoltage.[77,78] Cheng *et al.* used P3HT:ICBA blends to fabricate inverted devices, introducing a nanostructured scattering rear electrode to enhance the light-trapping efficiency.[78] The Ag NPs were fabricated through thermal deposition and sandwiched between MoO_3 layers, resulting in an interesting device structure: ITO/ZnO/P3HT:ICBA/MoO_3/Ag NPs/MoO_3/Al. The PCE increased to 7.21% from a value of 6.26% for the reference cell prepared without plasmonic NPs at the electrode.

A single organic material can only absorb within a limited range of the solar spectrum. To extend the absorption region, many low-band gap (LBG) polymers have been developed to harvest low-energy photons from solar irradiation. For example, polythieno[3,4-*b*]thiophene/benzodithiophene (PTB7) is one of the most promising LBG polymers; a PCE of over 7% has been achieved for a device based on a PTB7:$PC_{70}BM$ polymer blend.[77] Metal NPs have also been employed to further improve the performance of OPVs incorporating these LBG polymers. Recently, Baek *et al.* investigated the effect of size-control by blending Ag NPs into the anodic PEDOT:PSS buffer; the photoactive layer was a blend of PTB7 and $PC_{70}BM$.[79] They compared the performance of the devices incorporating various particle sizes, with the PCE of the optimal PTB7-based device increasing to 8.6%. Meanwhile, Choi *et al.* reported a PTB7:$PC_{70}BM$ device exhibiting an impressive efficiency of 8.92%.[80] As displayed in Fig. 4(a), they prepared silica-coated silver (Ag@SiO_2) NPs and incorporated them into devices to trigger LSPR effects. The Ag@SiO_2 NPs were either blended directly into the PEDOT:PSS layer (type I) or positioned at the interface between the PEDOT:PSS and the photoactive layer (type II) [Fig. 4(b)]. In the type II architecture, the presence of the silica shells avoided possible exciton quenching by preventing direct contact between the Ag cores and the active layer. Choi *et al.* found that both types of structures led to improved device efficiencies. They concluded that the multipositional and solution-processable properties of core/shell NPs offer the possibility of providing plasmonic effects when introducing these nanomaterials into various spatial locations.[80] More recently, another interesting type of plasmonic Ag NPs was demonstrated. Choi *et al.* prepared carbon dot-supported Ag NPs (CD–Ag NPs) and used them in the fabrication of solution-processable polymer optoelectronic devices.[81] The electron-donating properties of UV-excited CDs enable rapid reduction of Ag salts to form Ag NPs on the surfaces of the CDs. The CD–Ag NPs had average diameters of approximately 6 nm for the CDs and approximately 3 nm for the Ag NPs. A broad light extinction occurred with a peak near 460 nm [Fig. 4(c)]. In

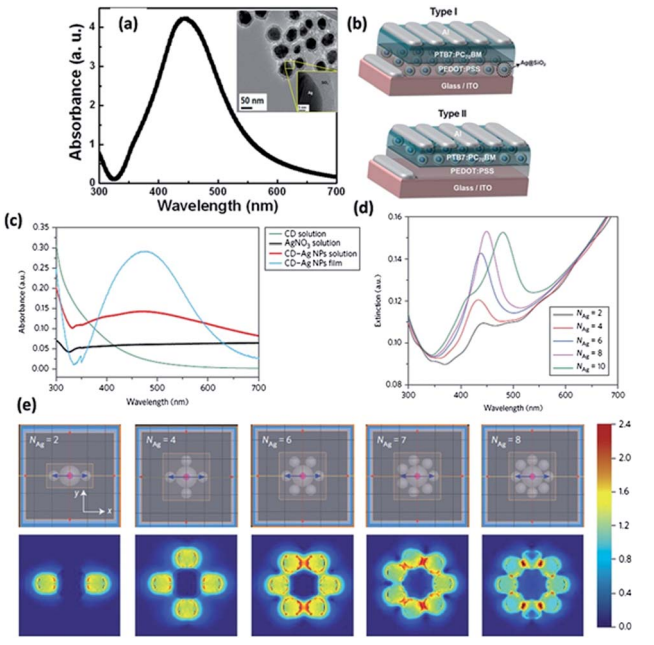

Fig. 4 Modified Ag NPs for use in plasmonic-enhanced OPVs. (a) Absorption spectrum and TEM image of Ag@SiO_2 NPs. (b) Structures of OPVs.[80] (c) Absorption spectra of as-prepared CD–Ag NPs in different forms. (d and e) Simulated (d) extinction spectrum and (e) electric field distribution for CD–Ag NPs, plotted with respect to the number of Ag NPs on the surface of the CDs (N_{Ag}). The magnitude of the enhancement in the electric field intensity is indicated by the colour scale.[81]

contrast, the peak absorption occurred near 420 nm for free Ag NPs having a similar diameter; thus, the plasmonic peak shifted by approximately 40 nm. This wavelength shift was simulated using the three-dimensional finite-difference time-domain (FDTD) method; Fig. 4(d) and (e) present the predicted extinction spectra and the simulated electrical field intensity distribution, respectively, plotted with respect to the number of Ag NPs (N_{Ag}) attached to the CD surfaces. Red-shifting of the spectra occurred upon increasing the value of N_{Ag}, with a strong field enhancement at the gaps between the NPs, suggesting a significant clustering effect of the NPs. The application of the CD–Ag NPs in OPVs, having a device structure of ITO/CD–Ag NP/PEDOT:PSS/PTB7:PC_{70}BM/Al, resulted in an improvement in PCE up to 8.31%, clearly demonstrating the potential of these templated Ag NPs.

The incorporation of two different NPs can lead to cooperative plasmonic effects. As displayed in Fig. 5(a), Lu *et al.* mixed Ag and Au NPs and then incorporated them into the anodic PEDOT:PSS buffer.[82] They obtained a high PCE of 8.67%, corresponding to a 20% enhancement of efficiencies. The dual NPs provided a broader absorption-enhancing range relative to that of either single type of NPs. UV-vis absorption spectra confirmed that the absorption efficiency of the PTB7:PC_{70}BM cell in the range from 420 to 600 nm was enhanced after adding Ag NPs; further incorporation of Au NPs increased the absorption efficiency in the wavelength range from 520 to 750 nm [Fig. 5(b)]. The two complementary resonance peaks of these two different types of NPs resulted in OPVs having a much broader light absorption enhancement region.

Alloy NPs have also employed for plasmonic-enhanced OPVs.[84,85] When a polystyrene-*block*-poly(2-vinylpyridine) (PS-*b*-P2VP) copolymer was used as a template for fabricating arrays of metal NPs on ITO substrates, metallic (Au and Cu) salts were blended and converted to either pure or alloy NPs.[84] For P3HT:PCBM BHJ systems having the device structure ITO/metal NP/PEDOT:PSS/P3HT:PCBM/Al, the PCE of the reference cell was 2.9%, improving to 2.98 and 3.22% when the Au and Cu NPs, respectively, were incorporated into the devices. For the device containing the Au–Cu alloy NPs, the efficiency improved even further to 3.35%.

3.1.2 Nanoparticles with non-spherical or abnormal shapes. While the majority of the existing studies on the plasmonic OPVs are focused on spherical nanoparticles, more and more recent articles study the shape effects of these plasmonic materials.[39,46,86–89] We recently introduced both Au NPs and nanorods (NRs) into the P3HT:PCBM devices and found improved light trapping efficiencies.[83] Tunable LSPR bands at different wavelength regions from 520 to 850 nm have been achieved through altering the sizes and shapes (Fig. 6). Because of the two different resonance modes along the short and long axes—classified as the transverse and longitudinal mode, respectively, a wide range of LSPR become possible. L. Lu *et al.* further proved that one single type Au NRs could also achieve a broad light absorption enhancement region due to their dual plasmonic bands along the two axes of the nanorods [Fig. 5(c)].[82] A PCE of 8.52% has been achieved for the device based on the PTB7:PC_{70}BM blends; this value is close to the PCE obtained using Ag and Au NP blends [Fig. 5(d)].[82]

Oo *et al.* synthesized ultrafine Au nanowires (NWs), using a solution-phase approach, for application as plasmonic antennae in P3HT:PCBM solar cells.[90] Fig. 7(a) illustrates their device structure; notably, a layer of PEDOT:PSS was incorporated as a spacer between the active layer and the Au NW network. The absorption of the device was enhanced over the spectral regime ranging from 400 to 700 nm. The photocurrent increased by 23.2% and the PCE was improved by 11.4%. Oo *et al.* concluded that a strong localized plasmon field and

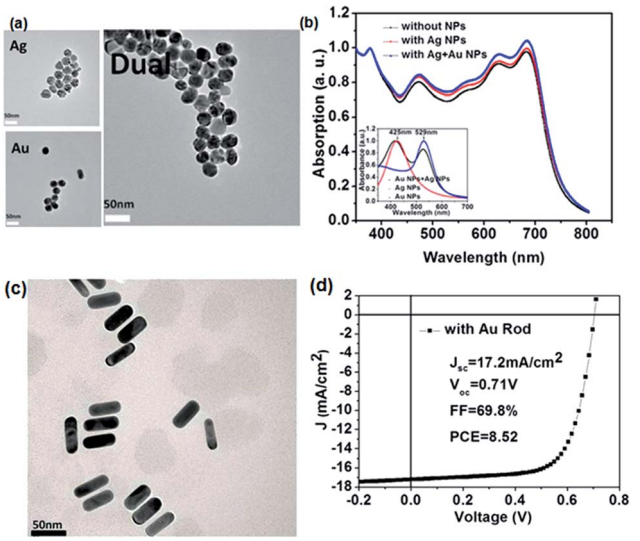

Fig. 5 Plasmonic nanostructures that result in broader absorption enhancement regimes.[82] (a) TEM images of Ag and Au NPs and their mixture. (b) UV-vis absorption spectra of PTB7:PC_{70}BM devices prepared with and without NPs; inset: absorption spectra of the NPs in water.[82] (c) TEM image of Au rods in water. (d) *J*–*V* curve of the PTB7:PC_{70}BM cell after Au NRs had been blended into the device.

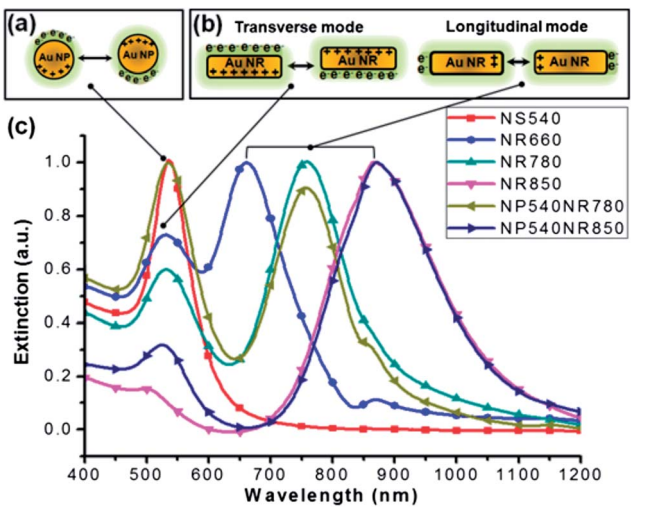

Fig. 6 (a and b) Dipolar oscillations in (a) spherical Au NPs and (b) Au NRs. (c) Normalized UV-vis-NIR absorption spectra of Au NPs of various sizes and shapes in water.[83]

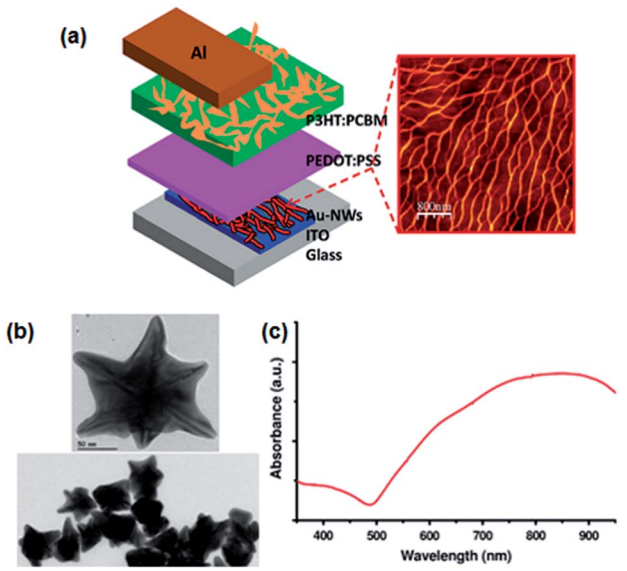

Fig. 7 Non-spherical NPs for plasmonic-enhanced OPVs. (a) The structure of an Au NW device and the high-resolution TEM image of as-synthesized ultrafine NWs.[90] (b) The TEM image of the nanostars. (c) The UV-vis absorption spectrum of the nanostar colloids in aqueous medium.[34]

increased far-field scattering collectively led to the enhancement in absorption. Furthermore, Kozanoglu *et al.* compared the SP effects of abnormally shaped particles with those of nanospheres.[34] NPs having sharp features should contribute to a greater extent to device enhancement because of their strong local electromagnetic fields.[91] Fig. 7(b) and (c) display TEM images and a corresponding UV-vis absorption spectrum, respectively, of the nanostars;[34] the tip-to-tip distance was approximately 150 nm. Because of the various resonance modes, a broad plasmon absorption band appeared, ranging from 500 to 900 nm. After NPs of various shapes—nanostars, nanorods, and nanospheres—had been doped into the PEDOT:PSS buffers of the devices based on P3HT:PCBM blends, the PCEs increased by approximately 29, 14, and 11%, respectively. Among the tested nanostructures, Au nanostars exhibited the highest field enhancement around the NPs, presumably because of their branched structures and sharp features.[34]

3.2 Metal NPs embedded into photoactive layers

In principle, directly embedding nanostructures into the photoactive layer would be a straightforward means of exploiting their plasmonic effects. From a theoretical point of view, Sha *et al.* developed a rigorous electrodynamic approach for investigating the optical absorption in OPVs; they observed remarkable differences between the behavior of metal NPs placed inside the interlayer between the active layer and the anode and those embedded directly into the photoactive layer.[92–94] The enhancement factors (Table 1) were generally higher when the NPs were blended directly into the active layer.[95] Nevertheless, the direct embedding method has many concerns, including possible exciton quenching and rapid charge recombination at

Table 1 Enhancement factors for metal NPs embedded into the spacer and the active layer[100]

	NP types	Vertical incidence	Oblique incidence
Spacer layer	Separated small	0.992	1.078
	Close-packed small	0.989	1.174
	Separated large	0.927	0.935
	Close-packed large	0.725	0.960
Active layer	Separated small	1.366	1.374
	Close-packed small	1.985	1.821
	Separated large	1.118	1.216
	Close-packed large	1.342	1.589

the surface of the metal NPs. As we will see in many examples below, serious phase separation between the nanostructures and the organic semiconductors also dampen their positive effects on device performance.

As early as 2004, Ag and Au NPs were directly doped into the photoactive layer of OPVs. Although the device efficiency was indeed improved, the authors concluded that the cell enhancement was due to the improved electrical conductivity.[54] In 2010, Xue *et al.* also embedded Ag NPs into the P3HT:PCBM layer, but did not observe significant device enhancement.[96] Although the mobility of the active layer increased, the number of total extracted carriers decreased. From an analysis of the surface morphology of the active layers, Xue *et al.* found that the Ag NPs tended to phase-segregate from the organic components. On the other hand, the formation of such an Ag NP subnetwork might explain the increased device mobility.[96] More recently, many successful examples regarding blending metal NPs into the photoactive layers have been reported.[97–99] Wang *et al.* added truncated octahedral Au NPs in the OPVs fabricated from P3HT/$PC_{70}BM$, poly[*N*-9′′-hepta-decanyl-2,7-carbazole-*alt*-5,5-(4′,7′-di-2-thienyl-2′,1′,3′-benzothiadiazole)] (PCDTBT)/$PC_{70}BM$, and poly{[4,4′-bis(2-ethylhexyl)dithieno(3,2-b:2′,3′-d) silole]-2,6-diyl-*alt*-[4,7-bis(2-thienyl-2,1,3-benzothiadiazole-5,5′-diyl)]} (Si-PCPDTBT)/$PC_{70}BM$, and found that the PCE increased from 3.54% to 4.36% for the devices based on P3HT/$PC_{70}BM$ blends.[97] For other polymer systems, the efficiencies were also improved from 5.77% to 6.45% (PCDTBT/$PC_{70}BM$), and from 3.92% to 4.54% (Si-PCPDTBT/$PC_{70}BM$). Because the average size of the truncated octahedral Au NPs was approximately 700 nm, Wang *et al.* suggested that multiple scattering, leading to longer optical paths within the active polymer materials, was responsible for the enhancement in the PCE. Furthermore, the lower series resistance extracted from the dark *J*–*V* curves indicated that improved charge transport also contributed to the device enhancement, because the Au NPs also behaved as hole conductors. Meanwhile, Ag NPs synthesized through solution polyol chemistry were also blended with the PCDTBT/$PC_{70}BM$ active layers; again, device enhancement was observed.[98]

Although surface coating of NPs can help to improve their dispersion in a polymer matrix, insulating layers might attenuate the plasmonic field, resulting in a less effective

Table 2 Device performance of the plasmonic-enhanced OPVs fabricated with NPs[a]

Plasmon scheme/active layer	J_{sc} (mA cm^{-2})	V_{oc} (V)	FF (%)	PCE (%)	Ref.
Ag nanoprism/P3HT:$PC_{61}BM$	1.99 (1.43)	0.50 (0.55)	52.3 (57.3)	5.21 (4.58)	30
Au@SiO_2 NR/PCPDTBT:$PC_{70}BM$	12.7 (11.4)	0.597 (0.597)	58.1 (51.4)	4.4 (3.5)	35
Inorganic NP/P3HT:$PC_{61}BM$	11.8 (10.1)	0.59 (0.59)	61 (59)	4.3 (3.5)	51
Au NP/P3HT:$PC_{61}BM$	10.22 (9.16)	0.59 (0.59)	70.32 (66.06)	4.24 (3.57)	54
Ag NP/P3HT:$PC_{61}BM$	6.9 (4.6)	0.581 (0.590)	—	2.2 (1.3)	55
Ag NP/P3HT:$PC_{61}BM$	—	—	55 (53)	3.69 (3.05)	58
Au NP/P3HT:$PC_{61}BM$	10.18 (8.95)	0.59 (0.59)	69.8 (65.9)	4.19 (3.48)	59
MoO_3 + Au NP/P3HT:$PC_{61}BM$	10.9 (10.2)	0.60 (0.60)	64 (60)	4.20 (3.68)	65
Cs_2CO_3 + Au NP/P3HT:$PC_{61}BM$	10.11 (9.73)	0.55 (0.55)	64 (59)	3.54 (3.12)	68
Au–GO/P3HT:$PC_{61}BM$	9.43 (8.46)	0.63 (0.60)	59.7 (51.5)	3.55 (2.79)	71
Au–GO/P3HT:$PC_{61}BM$	10.44 (8.87)	0.57 (0.57)	66.8 (64.5)	3.98 (3.26)	74
Au–GO/P3HT:ICBA	9.94 (8.61)	0.81 (0.81)	62.7 (57.7)	5.05 (4.02)	
MoO_3–Ag NP/P3HT:ICBA	12.86 (11.64)	0.85 (0.84)	66 (64)	7.21 (6.26)	78
Ag NP/PCDTBT	12.67 (11.22)	0.89 (0.89)	67 (64)	7.6 (6.4)	79
Ag NP/PTB7:$PC_{70}BM$	16.33 (14.93)	0.75 (0.75)	70 (70)	8.6 (7.9)	
Ag@SiO_2/PTB7:$PC_{70}BM$	16.65 (14.64)	0.74 (0.74)	68 (67)	8.49 (7.26)	80
Dual Au + Ag NP/PTB7:$PC_{71}BM$	17.7 (15.0)	0.71 (0.72)	69.0 (67.1)	8.67 (7.25)	82
Dual Au NP + NR/P3HT:$PC_{60}BM$	11.49 (9.28)	0.59 (0.59)	63 (64)	4.28 (3.46)	83
Dual Au + Cu NP/P3HT:$PC_{61}BM$	9.37 (8.08)	0.58 (0.60)	61 (60)	3.35 (2.90)	84
AuAg alloy NP/P3HT:$PC_{61}BM$	12.21 (10.12)	0.63 (0.61)	61.5 (58.4)	4.73 (3.61)	85
Dual Ag NP + nanoprisim/P3HT:$PC_{61}BM$	10.61 (8.99)	0.64 (0.64)	63.33 (62.33)	4.3 (3.6)	86
Au NW/P3HT:$PC_{61}BM$	9.02 (7.87)	0.65 (0.65)	46 (48)	2.72 (2.44)	90
Au NP/P3HT:$PC_{70}BM$	11.18 (—)	0.63 (—)	61 (—)	4.36 (3.54)	97
Au NP/PCDTBT:$PC_{70}BM$	11.16 (—)	0.89 (—)	65 (—)	6.45 (5.77)	
Au NP/Si–PCPDTBT:$PC_{70}BM$	13.13 (—)	0.57 (—)	61 (—)	4.54 (3.92)	
Ag NP/PCDTBT:$PC_{70}BM$	11.61 (10.79)	0.86 (—)	69 (68)	7.1 (6.3)	98
Au NP/P3HT:$PC_{61}BM$	9.77 (8.27)	0.6 (0.6)	63.38 (53.22)	3.71 (2.64)	99
Al NP/P3HT:$PC_{61}BM$	11.31 (8.59)	0.6 (0.6)	59 (61)	4.00 (3.14)	101
Au–Al NP/PCDTBT:$PC_{61}BM$	12.71 (11.27)	0.86 (0.86)	56 (55)	6.12 (5.33)	102
Au NP/tandem, P3HT:ICBA–PSBTBT:$PC_{70}BM$	6.92 (6.06)	1.457 (1.455)	61.91 (59.22)	6.24 (5.22)	104
Au NP/MEH–PPV:$PC_{61}BM$	*I_{sc} (mA), 74.39 (66.79)	0.78 (0.76)	44.8 (39.2)	2.36 (1.99)	105
Au NP/PFSDCN:$PC_{61}BM$	—	—	—	2.17 (1.64)	106
Ag NP/PCDTBT:$PC_{71}BM$	12.12 (11.63)	0.87 (0.90)	61 (57)	6.4 (5.9)	107
Ag nanoplate/PCDTBT:$PC_{71}BM$	13.19 (11.63)	0.87 (0.90)	57 (57)	6.6 (5.9)	
Ag NP/P3HT:$PC_{71}BM$	9.33 (7.89)	0.58 (0.59)	53 (52)	2.82 (2.41)	108
Pt NP/P3HT:$PC_{61}BM$	8.54 (9.53)	0.57 (0.53)	52.8 (45.3)	2.57 (2.29)	109
Au NP/P3HT:$PC_{61}BM$	9.74 (8.35)	0.61 (0.61)	65.00 (61.92)	3.85 (3.16)	110
Dual Ag nanodots + NP/P3HT:$PC_{61}BM$	11.20 (9.21)	0.64 (0.63)	67.0 (69.3)	4.80 (4.02)	111
Au@SiO_2/P3HT:$PC_{61}BM$	10.6 (10.0)	0.62 (0.61)	57 (54)	3.80 (3.29)	112
MoO_3–Ag NP/PCDTBT:$PC_{70}BM$	10.43 (9.12)	0.88 (0.88)	64 (64)	5.87 (5.07)	113
Ag NP/PCDTBT:$PC_{70}BM$	10.10 (9.18)	0.89 (0.89)	61 (62)	5.57 (5.08)	

[a] The dash mark (—): data not provided; numbers in parentheses: data from reference devices.

enhancement in absorption. Spyropoulos *et al.* embedded surfactant-free Au NPs, synthesized through ultrafast laser ablation in liquids, into a P3HT:PCBM layer; they found that the PCE improved by 40%,[99] suggesting that the uncoated surface of the NPs could eliminate recombination pathways. In addition to noble metals, other metals, including Al (ref. 101–103) and Cu,[84] have also been tested as promising candidates for improving the performance of OPVs. Kochergin *et al.* found that Al NPs are especially suitable for use in organic materials because Al has a higher plasma frequency, which ensures better overlap between its resonance peaks and the absorption band of the organic semiconductors.[103] Kakavelakis *et al.* further demonstrated enhancements in both device efficiencies and stability when using Al NPs generated through laser ablation.[101] The Al NPs behaved as effective optical reflectors, allowing the solar radiation to pass multiple times through the P3HT:PCBM active layer. The value of J_{sc} increased by 31.66%—from 8.59 to 11.31 mA cm^{-2}—after incorporation of the Al NPs, while the PCE improved from 3.14 to 4.00%. More interestingly, stability tests indicated that the degradation rate of the Al NP-doped device was much slower than those of standard devices. Kakavelakis *et al.* attributed the better device stability to the efficient quenching of triplets, thereby inhibiting photooxidation processes within the devices.[101] Furthermore, when Au–Ag alloy NPs were synthesized in organic media using a one-pot reaction,[85] the efficiency of the P3HT:PCBM device increased to 4.37%—a 31% enhancement—after doping the alloy NPs into the active layer. Chen *et al.* attributed the improved device performance to enhanced light trapping and better charge transport in the active layer. The device performance of the plasmonic-enhanced OPVs fabricated with NPs is summarized in Table 2.

3.3 Periodic metallic nanostructures

Another promising strategy for enhancing the performance of OPVs is to use periodic metal nanostructures, which can usually fulfill the momentum mismatch conditions, as described in the previous section. While the preparation of metal NPs seems to be a simpler approach, it is difficult to precisely control their sizes, shapes, and, most importantly, monodispersity; manipulating their distribution within devices is also very challenging. By tuning the geometrical factors of periodic nanostructures, the resonance wavelength of the SPP modes can be tuned readily within the visible to near-infrared (NIR) spectral range.[29,38–41,114–120] Furthermore, these structures are also easier to model, facilitating theoretical studies. For instance, Tvingstedt *et al.* constructed periodic Al gratings to induce propagating plasmons; Fig. 8(a) illustrates the device structure.[43] They used the grating as the bottom cathode and deposited two different polymers (APFO3, APFO Green5) containing PCBM molecules as active layers; a layer of PEDOT:PSS served as the top anode. Fig. 8(b) and (c) display the corresponding absorption spectra measured in different polarization directions. The absorption spectra were different from those of the planar structure. In addition, different absorption patterns were observed when the devices were illuminated with differently directed polarized light. The results suggested that the transverse-electric (TE) polarized electromagnetic wave could not excite the plasmons. The IPCE spectra of the devices also revealed apparent polarization effects depending on the direction of the spectra, implying that the propagating plasmons could indeed increase the photocurrent. A successful example of a grating structure was reported by You *et al.* in 2012.[121] Their metal grating back electrode was implemented using an imprinting technique [Fig. 8(d)]. After patterning the devices, the PCE increased from 7.20 to 7.73% when using an LBG polymer (PTB7) as the active polymer.

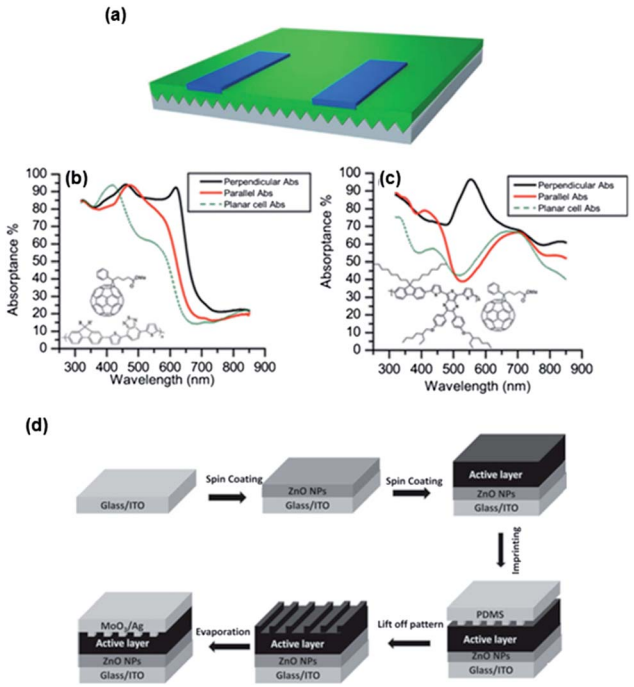

Fig. 8 (a) Periodic grating structure, shown in the middle, for supporting the propagating SPs. The polymer materials were sandwiched between the Al grating cathode and the PEDOT:PSS top anode. (b and c) Absorption spectra of (b) APFO3/PCBM and (c) APFO Green5/PCBM polymer blends on the grating structures, recorded with illumination from various polarization directions.[43] (d) Processing flow of the patterned polymer solar cells.[121]

One-dimensional (1D) grating structures often have high polarization-dependence, usually limiting their application in photovoltaic devices because of the randomly polarized nature of solar radiation. Sefunc *et al.* proposed and simulated both 1D and two-dimensional (2D) metal gratings for OPVs based on P3HT:PCBM blends, finding that the absorption efficiency could be increased by approximately 21% in all polarizations.[122] Through FDTD numerical calculations, Kim *et al.* identified multiple SP modes for Ag grids in ultrathin OPVs.[100] They attributed the absorption enhancements in the OPVs incorporating the metal grids to both the SPP mode excited at the glass–Ag interface and the LSP mode of the metal grids. They also found another SPP mode at the interface between the metal and the active layer after incorporation of 2D grids (Fig. 9). Indeed, light trapping significantly differs between the TE and transverse-magnetic (TM) modes for 1D gratings. Nevertheless, 2D or quasi-3D structures, possessing higher-order symmetries, offer

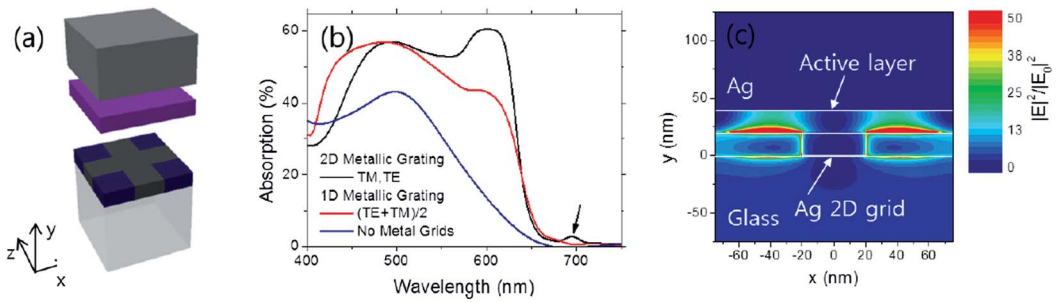

Fig. 9 (a) Schematic representation of a device structure featuring a 2D metal grid embedded in a buffer layer. (b) Absorption spectra of cells prepared with and without 1D and 2D metal grids, recorded under randomly polarized light; width and period of the metal grids: 40 and 150 nm, respectively. (c) Normalized E-field intensity distributions at a wavelength of 695 nm under polarized light in the *x* direction; the contour plot is displayed on the cross-section along the *x*–*y* plane passing through the vertical interface between the metal grid and the buffer layer.[100]

the opportunity for further optimization of the optical absorption. Broadband absorption enhancement over the entire solar spectrum can also be potentially realized when using 2D metal grids.

Several plasmonic architectures have been employed to prepare nanostructures with higher-order symmetries.[44,89,115,117,119,123] Dunbar *et al.* fabricated Ag nanovoid arrays, through nano-imprinting on both $PC_{61}BM$ and PCPDTBT:$PC_{61}BM$ layers;[115] they observed optical absorbing enhancements of up to approximately 80 and 40%, respectively, for these films. For practical applications, Kirkeminde *et al.* prepared Au plasmonic nanopyramid (NPY) structures, through self-assembled lithography, onto the substrates of silole-thiophene conjugated polymer (P3):$PC_{61}BM$ devices.[89] They fabricated polystyrene (PS) nanospheres of various sizes as templates on an ITO substrate [Fig. 10(c)]; these tightly coordinated PS spheres behaved as excellent templates for NPYs with sharp tips and edges, enabling enhanced plasmonic resonance. Au NPY arrays, uniform in size and distribution, were obtained after evaporating a 30 nm Au film and removing the PS spheres through a lift-off process [Fig. 10(a)]. Fig. 10(e) presents the absorption spectra of the Au NPY arrays and the photoactive layer; the 110 nm side-length Au NPYs exhibited the most suitable plasmon resonance for effective coupling with the P3:$PC_{61}BM$ photoabsorption. A 50% increase in photocurrent was measured, with the average current density improving from 2.7 ± 0.2 to 4.1 ± 0.3 mA cm^{-2}; the average PCE ($1.10 \pm 0.05\%$) was approximately 200% greater than that of the device prepared without the NPY arrays ($0.36 \pm 0.02\%$). Meanwhile, Wu *et al.* fabricated large-area periodic Ag nanotriangle (NT) arrays [Fig. 10(d)] through self-assembled nanosphere lithography in PCDTBT:PCBM devices.[116] The hexagonal NT arrays increased the absorption efficiency and improved the device PCE from 4.24 to 4.52%, presumably because of greater exciton generation induced by the strong local electric field and the SP-induced scattering.

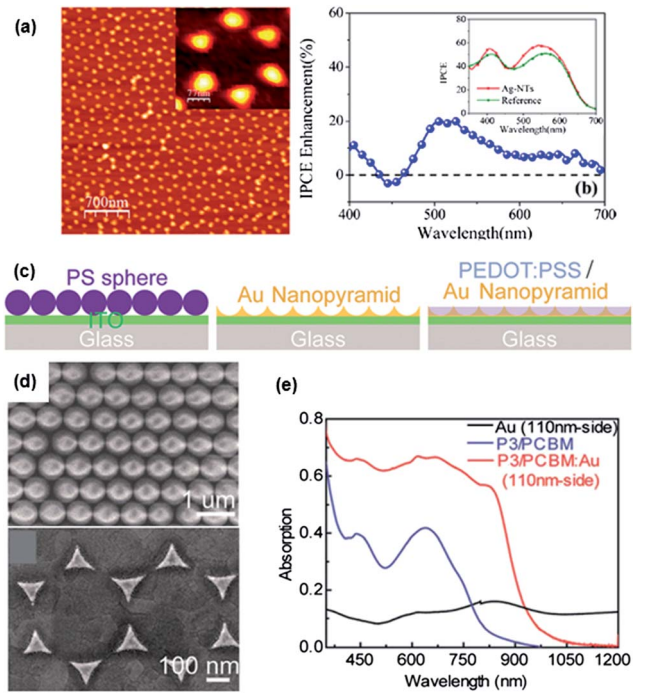

Fig. 10 Nanostructures with higher-order symmetries. (a) AFM images of the Ag–NT arrays. The height and size of the triangles are *ca.* 20 and 40 nm, respectively. The inset shows a zoom-in unit of the NT array. (b) Percentage enhancement in the IPCE of the devices with NTs. The inset shows the corresponding IPCE spectra of the two devices.[116] (c) The self-assembled PS sphere nanolithography to prepare Au NPY arrays. The structure was then covered with PEDOT:PSS for device fabrication. (d) SEM images of the PS spheres (up) and Au NPYs with 110 nm side-length (down). (e) The absorptions of Au NPYs, P3/$PC_{61}BM$, and Au NPY plasmonic enhanced OPV.[89] Reproduced from ref. 89.

3.4 Dual plasmonic nanostructures

Many conventional plasmonic nanostructures, such as spherical NPs, can cover only a narrow spectral bandwidth; therefore, a single structure alone cannot harvest the broad spectrum of solar radiation. Furthermore, different nanostructures present different functionalities and operate through different device-enhancing mechanisms when incorporated at different positions, as we have seen above. Therefore, many researchers have tested the effects of incorporating pairs of different plasmonic structures simultaneously in a single device (Table 3). For example, Xie *et al.* synthesized poly(ethylene glycol)

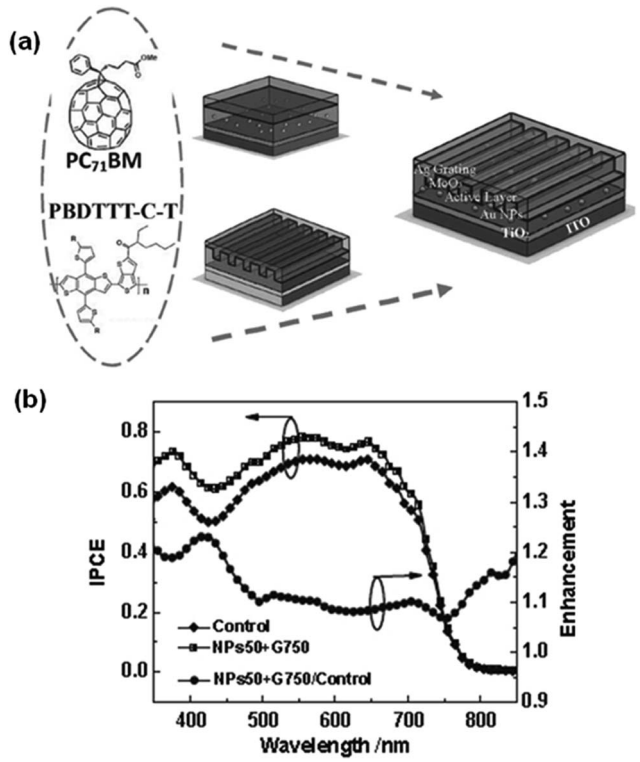

Fig. 11 (a) Chemical structures of PBDTTT-C-T and $PC_{71}BM$ (left). Schematic representation of the device structure: NP device (top), grating device (bottom), and dual metallic structures (right) (b) The IPCE spectra of the control (flat) and the optimized devices. The enhancement factor is also plotted.[124]

Table 3 Device performance of the plasmonic-enhanced OPVs fabricated with periodic nanostructures[a]

Plasmon scheme/active layer	J_{sc} (mA cm^{-2})	V_{oc} (V)	FF (%)	PCE (%)	Ref.
Au NPY/P3:$PC_{61}BM$	4.1 (2.7)	—	—	1.10 (0.36)	89
Au:SH–PEG NPY/P3:$PC_{61}BM$	—	—	—	1.1 (0.84)	
Ag NT array/PCDTBT:$PC_{61}BM$	9.57 (8.55)	4.52 (4.24)	53 (55)	4.52 (4.24)	116
Al nanodisk array/PCPDTBT:$PC_{60}BM$	—	—	—	4.52 (—)	117
Ag nanograting/PTB7:$PC_{71}BM$	15.50 (14.05)	0.720 (0.726)	69.08 (70.62)	7.73 (7.20)	121
Au NPs + Ag nanograting/PBDTTT-C-T:$PC_{71}BM$	18.39 (17.09)	0.76 (0.76)	62.87 (58.43)	8.79 (7.59)	124
MoO_x/Ag nanoporous film/SubPc-C_{60}	5.15 (5.43)	1.03 (1.04)	65.03 (62.19)	3.45 (3.51)	127
Corrugated Au–Al electrode/CuPc-C_{60}	5.5 (4.1)	0.46 (0.46)	57 (57)	1.44 (1.07)	128

[a] The dash mark (—): data not provided; numbers in parentheses: data from reference devices.

(PEG)-capped Au NPs and positioned them into both the PEDOT:PSS buffer and the active layer.[110] They demonstrated the accumulated benefits of incorporating these NPs into all polymer layers. The Au NPs in the PEDOT:PSS layer contributed mainly to improved hole collection, while those in the active layer enhanced the optical absorption and helped to balance charge transport. Li *et al.* combined two different approaches—blending metal NPs and using 1D grating backcontacts—to improve the device efficiencies in inverted OPVs incorporating a blend of poly{[4,8-bis(2-ethylhexylthien-5-yl)benzo[1,2-*b*:4,5-*b*′]-dithien-2,6-diyl]-*alt*-[2-(2′-ethylhexanoyl)thieno[3,4-*b*]thien-4,6-diyl]}(PBDTTT-C-T) and $PC_{71}BM$ as the active later.[124]

Fig. 11(a) presents the device structure and the chemical structures of the component materials. The flat control device, fabricated without any nanostructures, exhibited a PCE of 7.59 ± 0.08%. Then, Au NPs having diameters of 20 and 50 nm were doped into the PBDTTT-C-T:$PC_{71}BM$ active layer. Meanwhile, Ag grating electrodes having periodicities of 750 and 350 nm were prepared, through vacuum-assisted nanoimprinting, as the back electrodes. For the best device, in which the grating interval was 750 nm, the PCE reached 8.38 ± 0.20%. After the Au NPs had also been added to the active layer, the PCE increased further to 8.79 ± 0.15%. Li *et al.* found that the Au NPs enhanced the device absorption in the spectral region from 480 to 600 nm, whereas the Ag grating had a greater impact on the absorptions in the regions below 400 nm and above 600 nm [Fig. 11(b)].[124] More recently, Liu *et al.* demonstrated the dual effects of Au nanodots (NDs) and NPs within OPVs.[111] They incorporated octahedral Au NPs within the hole transport layer (PEDOT:PSS) and thermally evaporated Au NDs onto the P3HT:PCBM active layer. The device PCE increased by 15% after positioning the Au NDs at the cathode interface and then increased further, by 20%, after including both nanostructures, indicating the great potential of using such an approach.

4 Conclusion and outlook

After tremendous progress made in the past decade, PCEs exceeding 10% have been achieved for single-junction OPVs. An earlier research study revealed that the internal quantum efficiencies of OPVs could approach almost 100%.[125,126] Hence, sufficient absorption of sunlight remains one of the limitations affecting the development of higher-efficiency devices. While many light trapping approaches have been proposed, the use of plasmonic nanostructures is one of the most promising routes toward harvesting more solar radiation. The optical properties of these nanostructures are simply tuned through structural design and material selection. Moreover, they are readily incorporated into OPVs. In this Article, we first discussed the fundamentals of SPs and described the three main categories of plasmonic nanostructures that have been used to enhance the performance of OPVs. We have reviewed the recent literature, highlighting the rapid progress in this field with a focus on studies of BHJ polymer-based solar cells. Using most of these approaches, the photocurrents and/or PCEs have frequently increased by 20–30%. The most simple and assessable method is the introduction of metal NPs in the vicinity of the photoactive layer—that is, in the buffer layer or at the organic–electrode interface. The plasmonic field, however, usually decays exponentially, resulting in limited near-field effects on the absorption enhancement of the photoactive layer. A less-simple, but rather straightforward method, is to directly embed the nanostructures in the semiconductor layer. The resulting morphology, however, should be carefully controlled because phase separation between the nanostructures and the organic materials can degrade the device. Furthermore, it is rather difficult to decouple the electrical and plasmonic effects of these nanostructures, at least under some experimental conditions. The use of periodic nanostructures is also a promising means of achieving positive plasmonic effects. These ordered architectures also simplify the structural design and are more amenable to theoretical investigations. Although 1D grating structures exhibit polarization dependence, some 1D nanostructures can provide certain benefits; 2D or even higher-order symmetries can be used to overcome such polarization issues. The high cost of fabrication of the periodic nanostructures, however, remains a challenge for future commercialization. In addition to improvements in efficiency, reliability is another important feature of a practical solar module. While some reports have demonstrated that the addition of metal NPs can improve the photostability, further efforts should be made to improve device stability.

The loading capacity of metal nanostructures in organic matrices is a very critical parameter in determining the device performance and should be further emphasized. Earlier reports

have indicated that a high concentration of metal nanoparticles tends to result in serious aggregation.[79,97,119] The clustering and/or stronger dipolar coupling between the particles might affect the plasmonic properties of the nanostructures.[79] As the metal surface probably quenches excitons and facilitates charge recombination, a high level of nanostructure loading could degrade the device performance. These loss mechanisms, however, are still not well understood yet, and needed to be elucidated. Further, controlled methods for the nanoparticle dispersion should be further developed. Together with the better understandings of the quenching mechanisms, the increased loading capacity might further benefit the device efficiencies.

Although many examples regarding the plasmonic-enhanced performance have been reported, in-depth understanding of the enhancement mechanism is still required. Theoretical studies and simulations are needed to support the existing experimental studies, especially for the rather complicated nanostructures, and to provide design rules for structure development in the further. The influence of the nanostructures on the electrical properties of the plasmonic-assisted OPVs is not clear yet. For example, the possibility of charge trapping on the metal NPs should be evaluated. Besides, the effect on the metal/organic interfaces of the nanostructures is another important concern.

In addition to conventional single-junction OPVs, plasmonic nanostructures have also been applied in other device architectures. Because the electrochemical potential of charge carrier extraction can be increased, tandem cell structures have been used widely to allow theoretical PCEs to surpass the Shockley–Queisser limit. Yang *et al.* incorporated Au NPs in the intermediate layer, which connects the two subcells, when building tandem OPVs.[104] The PCE increased by approximately 20%, revealing the great potential of the exploiting the plasmonic effect. We anticipate that many more device structures will be designed for ready incorporation of nanostructures. It is also worth noting that core/shell metal NPs have been employed recently in emerging meso-superstructured solar cells based on perovskite materials.[129] Because thin film-type perovskite solar cells have been demonstrated as efficient,[130] we expect the knowledge gained from studies of plasmonic-assisted OPVs to also benefit in enhancing the efficiencies of these emerging solar technologies.

In conclusion, plasmonic light trapping technologies have great potential for achieving high degrees of photon absorption in OPVs. Dennler *et al.* proposed that a PCE of approximately 15% might be possible through the development of multi-junction OPVs.[76] We believe that plasmonic nanostructures will play an important role in pushing the record PCE toward these theoretical predications. Finally, in addition to their attractive properties of light weight and high flexibility, we foresee that inexpensive, highly efficient, large-area OPV modules will be delivered in the near future.

References

1 K. Branker, M. J. M. Pathak and J. M. Pearce, *Renewable Sustainable Energy Rev.*, 2011, **15**, 4470–4482.
2 M. Kaltenbrunner, M. S. White, E. D. Głowacki, T. Sekitani, T. Someya, N. S. Sariciftci and S. Bauer, *Nat. Commun.*, 2012, **3**, 770.
3 Z. Liu, J. Li and F. Yan, *Adv. Mater.*, 2013, **25**, 4296–4301.
4 A. L. Roes, E. A. Alsema, K. Blok and M. K. Patel, *Prog. Photovolt: Res. Appl.*, 2009, **17**, 372–393.
5 A. J. Heeger, *Adv. Mater.*, 2014, **26**, 10–28.
6 Z. He, C. Zhong, S. Su, M. Xu, H. Wu and Y. Cao, *Nat. Photonics*, 2012, **6**, 591–595.
7 M. C. Scharber and N. S. Sariciftci, *Prog. Polym. Sci.*, 2013, **38**, 1929–1940.
8 J. You, C.-C. Chen, Z. Hong, K. Yoshimura, K. Ohya, R. Xu, S. Ye, J. Gao, G. Li and Y. Yang, *Adv. Mater.*, 2013, **25**, 3973–3978.
9 J. You, L. Dou, K. Yoshimura, T. Kato, K. Ohya, T. Moriarty, K. Emery, C.-C. Chen, J. Gao, G. Li and Y. Yang, *Nat. Commun.*, 2013, **4**, 1446.
10 J. You, L. Dou, Z. Hong, G. Li and Y. Yang, *Prog. Polym. Sci.*, 2013, **38**, 1909–1928.
11 Research Cell Efficiency Records, http://www.nrel.gov/ncpv/images/efficiency_chart.jpg.
12 M. A. Green, K. Emery, Y. Hishikawa, W. Warta and E. D. Dunlop, *Prog. Photovolt: Res. Appl.*, 2014, **22**, 1–9.
13 Q. Tai, J. Li, Z. Liu, Z. Sun, X. Zhao and F. Yan, *J. Mater. Chem.*, 2011, **21**, 6848–6853.
14 H. Hoppe and N. S. Sariciftci, *J. Mater. Res.*, 2004, **19**, 1924–1945.
15 A. Moliton and J.-M. Nunzi, *Polym. Int.*, 2006, **55**, 583–600.
16 Z. Liu, J. Li, Z.-H. Sun, G. Tai, S.-P. Lau and F. Yan, *ACS Nano*, 2012, **6**, 810–818.
17 J. Y. Kim, S. H. Kim, H. H. Lee, K. Lee, W. Ma, X. Gong and A. J. Heeger, *Adv. Mater.*, 2006, **18**, 572–576.
18 B. V. Andersson, D. M. Huang, A. J. Moule and O. Inganas, *Appl. Phys. Lett.*, 2009, **94**, 043302.
19 Y. Zhang, A. K. Pandey, C. Tao, Y. Fang, H. Jin, P. L. Burn and P. Meredith, *Appl. Phys. Lett.*, 2013, **102**, 013302.
20 F.-C. Chen, J.-L. Wu and Y. Hung, *Appl. Phys. Lett.*, 2010, **96**, 193304.
21 J. R. Tumbleston, D.-H. Ko, E. T. Samulski and R. Lopez, *Opt. Express*, 2009, **17**, 7670–7681.
22 D.-H. Ko, J. R. Tumbleston, A. Gadisa, M. Aryal, Y. Liu, R. Lopez and E. T. Samulski, *J. Mater. Chem.*, 2011, **21**, 16293–16303.
23 Y. Zhou, F. Zhang, K. Tvingstedt, W. Tian and O. Inganäs, *Appl. Phys. Lett.*, 2008, **93**, 033302.
24 H. A. Atwater and A. Polman, *Nat. Mater.*, 2010, **9**, 205–213.
25 E. Stratakis and E. Kymakis, *Mater. Today*, 2013, **16**, 133–146.
26 S. Pillai and M. A. Green, in *Comprehensive Renewable Energy*, ed. S. Ali, Elsevier, Oxford, 2012, pp. 641–656.
27 M. E. Tasgn, *Nanoscale*, 2013, **5**, 8616–8624.
28 M. Faraday, *Philos. Trans. R. Soc. London*, 1857, **147**, 145–181.
29 G. Armelles, J. B. González-Díaz, A. García-Martín, J. M. García-Martín, A. Cebollada, M. U. González, S. Acimovic, J. Cesario, R. Quidant and G. Badenes, *Opt. Express*, 2008, **16**, 16104–16112.

30 H. S. Noh, E. H. Cho, H. M. Kim, Y. D. Han and J. Joo, *Org. Electron.*, 2013, **14**, 278–285.
31 B. Gao, M. J. Rozin and A. R. Tao, *Nanoscale*, 2013, **5**, 5677–5691.
32 K. C. Vernon, A. M. Funston, C. Novo, D. E. Gómez, P. Mulvaney and T. J. Davis, *Nano Lett.*, 2010, **10**, 2080–2086.
33 Q. Xu, F. Liu, Y. Liu, K. Cui, X. Feng, W. Zhang and Y. Huang, *Sci. Rep.*, 2013, **3**, 2112.
34 D. Kozanoglu, D. H. Apaydin, A. Cirpan and E. N. Esenturk, *Org. Electron.*, 2013, **14**, 1720–1727.
35 X. Xu, A. K. K. Kyaw, B. Peng, D. Zhao, T. K. S. Wong, Q. Xiong, X. W. Sun and A. J. Heeger, *Org. Electron.*, 2013, **14**, 2360–2368.
36 K. Flomin, I. Jen-La Plante, B. Moshofsky, M. Diab and T. Mokari, *Nanoscale*, 2014, **6**, 1335–1339.
37 V. Kulkarni, E. Prodan and P. Nordlander, *Nano Lett.*, 2013, **13**, 5873–5879.
38 J. Braun, B. Gompf, G. Kobiela and M. Dressel, *Phys. Rev. Lett.*, 2009, **103**, 203901.
39 S. Lee, J. Shin, Y.-H. Lee and J.-K. Park, *ACS Nano*, 2010, **4**, 7175–7184.
40 S. Xiao and N. A. Mortensen, *Opt. Lett.*, 2011, **36**, 37–39.
41 Q. Lin, B. Hua, S.-F. Leung, X. Duan and Z. Fan, *ACS Nano*, 2013, **7**, 2725–2732.
42 B. Hua, B. Wang, M. Yu, P. W. Leu and Z. Fan, *Nano Energy*, 2013, **2**, 951–957.
43 K. Tvingstedt, N.-K. Persson, O. Inganas, A. Rahachou and I. V. Zozoulenko, *Appl. Phys. Lett.*, 2007, **91**, 113514.
44 E. Lee and C. Kim, *Opt. Express*, 2012, **20**, A740–A753.
45 M. C. Günendi, I. Tanyeli, G. B. Akgüç, A. Bek, R. Turan and O. Gülseren, *Opt. Express*, 2013, **21**, 18344–18353.
46 K. L. Kelly, E. Coronado, L. L. Zhao and G. C. Schatz, *J. Phys. Chem. B*, 2002, **107**, 668–677.
47 W.-Y. Chen, C.-H. Lin and W.-T. Chen, *Nanoscale*, 2013, **5**, 9950–9956.
48 V. E. Ferry, J. N. Munday and H. A. Atwater, *Adv. Mater.*, 2010, **22**, 4794–4808.
49 W. L. Barnes, A. Dereux and T. W. Ebbesen, *Nature*, 2003, **424**, 824–830.
50 S. A. Maier and H. A. Atwater, *J. Appl. Phys.*, 2005, **98**, 011101.
51 H.-C. Liao, C.-S. Tsao, T.-H. Lin, M.-H. Jao, C.-M. Chuang, S.-Y. Chang, Y.-C. Huang, Y.-T. Shao, C.-Y. Chen, C.-J. Su, U. S. Jeng, Y.-F. Chen and W.-F. Su, *ACS Nano*, 2012, **6**, 1657–1666.
52 K. D. G. I. Jayawardena, L. J. Rozanski, C. A. Mills, M. J. Beliatis, N. A. Nismy and S. R. P. Silva, *Nanoscale*, 2013, **5**, 8411–8427.
53 Q. Gan, F. J. Bartoli and Z. H. Kafafi, *Adv. Mater.*, 2013, **25**, 2385–2396.
54 J.-L. Wu, F.-C. Chen, Y.-S. Hsiao, F.-C. Chien, P. Chen, C.-H. Kuo, M. H. Huang and C.-S. Hsu, *ACS Nano*, 2011, **5**, 959–967.
55 A. J. Morfa, K. L. Rowlen, T. H. Reilly, M. J. Romero and J. van de Lagemaat, *Appl. Phys. Lett.*, 2008, **92**, 013504.
56 M. Ghanem, J. Singh, A. Al-Mayouf, M. Shaddad, M. Al-Hoshan and A. Al-Suhybani, *Electrocatalysis*, 2013, **4**, 134–143.
57 K. Xie, L. Sun, C. Wang, Y. Lai, M. Wang, H. Chen and C. Lin, *Electrochim. Acta*, 2010, **55**, 7211–7218.
58 S.-S. Kim, S.-I. Na, J. Jo, D.-Y. Kim and Y.-C. Nah, *Appl. Phys. Lett.*, 2008, **93**, 073307.
59 F.-C. Chen, J.-L. Wu, C.-L. Lee, Y. Hong, C.-H. Kuo and M. H. Huang, *Appl. Phys. Lett.*, 2009, **95**, 013305.
60 H. Xia, S. Bai, J. r. Hartmann and D. Wang, *Langmuir*, 2009, **26**, 3585–3589.
61 A. V. Stanishevsky, H. Williamson, H. Yockell-Lelievre, L. Rast and A. M. Ritcey, *J. Nanosci. Nanotechnol.*, 2006, **6**, 2013–2017.
62 J.-H. Huang, F.-C. Chien, P. Chen, K.-C. Ho and C.-W. Chu, *Anal. Chem.*, 2010, **82**, 1669–1673.
63 M. Jørgensen, K. Norrman and F. C. Krebs, *Sol. Energy Mater. Sol. Cells*, 2008, **92**, 686–714.
64 S. Murase and Y. Yang, *Adv. Mater.*, 2012, **24**, 2459–2462.
65 K.-S. Tan, M.-K. Chuang, F.-C. Chen and C.-S. Hsu, *ACS Appl. Mater. Interfaces*, 2013, **5**, 12419–12424.
66 S. K. Hau, H.-L. Yip, N. S. Baek, J. Zou, K. O'Malley and A. K.-Y. Jen, *Appl. Phys. Lett.*, 2008, **92**, 253301.
67 C. Tao, S. Ruan, X. Zhang, G. Xie, L. Shen, X. Kong, W. Dong, C. Liu and W. Chen, *Appl. Phys. Lett.*, 2008, **93**, 193307.
68 C.-S. Kao, F.-C. Chen, C.-W. Liao, M. H. Huang and C.-S. Hsu, *Appl. Phys. Lett.*, 2012, **101**, 193902.
69 P.-P. Cheng, G.-F. Ma, J. Li, Y. Xiao, Z.-Q. Xu, G.-Q. Fan, Y.-Q. Li, S.-T. Lee and J.-X. Tang, *J. Mater. Chem.*, 2012, **22**, 22781–22787.
70 V. Kumar and H. Wang, *Org. Electron.*, 2013, **14**, 560–568.
71 G.-Q. Fan, Q.-Q. Zhuo, J.-J. Zhu, Z.-Q. Xu, P.-P. Cheng, Y.-Q. Li, X.-H. Sun, S.-T. Lee and J.-X. Tang, *J. Mater. Chem.*, 2012, **22**, 15614–15619.
72 S.-S. Li, K.-H. Tu, C.-C. Lin, C.-W. Chen and M. Chhowalla, *ACS Nano*, 2010, **4**, 3169–3174.
73 J.-M. Yun, J.-S. Yeo, J. Kim, H.-G. Jeong, D.-Y. Kim, Y.-J. Noh, S.-S. Kim, B.-C. Ku and S.-I. Na, *Adv. Mater.*, 2011, **23**, 4923–4928.
74 M.-K. Chuang, S.-W. Lin, F.-C. Chen, C.-W. Chu and C.-S. Hsu, *Nanoscale*, 2014, **6**, 1573–1579.
75 M. C. Scharber, D. Mühlbacher, M. Koppe, P. Denk, C. Waldauf, A. J. Heeger and C. J. Brabec, *Adv. Mater.*, 2006, **18**, 789–794.
76 G. Dennler, M. C. Scharber, T. Ameri, P. Denk, K. Forberich, C. Waldauf and C. J. Brabec, *Adv. Mater.*, 2008, **20**, 579–583.
77 Y. Liang, Z. Xu, J. Xia, S.-T. Tsai, Y. Wu, G. Li, C. Ray and L. Yu, *Adv. Mater.*, 2010, **22**, E135–E138.
78 P.-P. Cheng, L. Zhou, J.-A. Li, Y.-Q. Li, S.-T. Lee and J.-X. Tang, *Org. Electron.*, 2013, **14**, 2158–2163.
79 S.-W. Baek, J. Noh, C.-H. Lee, B. Kim, M.-K. Seo and J.-Y. Lee, *Sci. Rep.*, 2013, **3**, 1726.
80 H. Choi, J.-P. Lee, S.-J. Ko, J.-W. Jung, H. Park, S. Yoo, O. Park, J.-R. Jeong, S. Park and J. Y. Kim, *Nano Lett.*, 2013, **13**, 2204–2208.
81 H. Choi, S.-J. Ko, Y. Choi, P. Joo, T. Kim, B. R. Lee, J.-W. Jung, H. J. Choi, M. Cha, J.-R. Jeong, I.-W. Hwang,

M. H. Song, B.-S. Kim and J. Y. Kim, *Nat. Photonics*, 2013, **7**, 732–738.
82 L. Lu, Z. Luo, T. Xu and L. Yu, *Nano Lett.*, 2012, **13**, 59–64.
83 Y.-S. Hsiao, S. Charan, F.-Y. Wu, F.-C. Chien, C.-W. Chu, P. Chen and F.-C. Chen, *J. Phys. Chem. C*, 2012, **116**, 20731–20737.
84 M. Heo, H. Cho, J.-W. Jung, J.-R. Jeong, S. Park and J. Y. Kim, *Adv. Mater.*, 2011, **23**, 5689–5693.
85 H.-C. Chen, S.-W. Chou, W.-H. Tseng, I. W. P. Chen, C.-C. Liu, C. Liu, C.-L. Liu, C.-h. Chen, C.-I. Wu and P.-T. Chou, *Adv. Funct. Mater.*, 2012, **22**, 3975–3984.
86 X. Li, W. C. H. Choy, H. Lu, W. E. I. Sha and A. H. P. Ho, *Adv. Funct. Mater.*, 2013, **23**, 2728–2735.
87 R. Jin, Y. Cao, C. A. Mirkin, K. L. Kelly, G. C. Schatz and J. G. Zheng, *Science*, 2001, **294**, 1901–1903.
88 C.-Y. Tsai, C.-Y. Wu, K.-H. Chang and P.-T. Lee, *Plasmonics*, 2013, **8**, 1011–1016.
89 A. Kirkeminde, M. Retsch, Q. Wang, G. Xu, R. Hui, J. Wu and S. Ren, *Nanoscale*, 2012, **4**, 4421–4425.
90 T. Z. Oo, N. Mathews, G. Xing, B. Wu, B. Xing, L. H. Wong, T. C. Sum and S. G. Mhaisalkar, *J. Phys. Chem. C*, 2012, **116**, 6453–6458.
91 E. Nalbant Esenturk and A. R. Hight Walker, *J. Raman Spectrosc.*, 2009, **40**, 86–91.
92 W. E. I. Sha, W. C. H. Choy, Y. P. Chen and W. C. Chew, *Opt. Express*, 2011, **19**, 15908–15918.
93 W. E. I. Sha, W. C. H. Choy and W. C. Chew, *Opt. Express*, 2010, **18**, 5993–6007.
94 W. E. I. Sha, W. C. H. Choy, Y. Wu and W. C. Chew, *Opt. Express*, 2012, **20**, 2572–2580.
95 W. E. I. Sha, W. C. H. Choy, Y. G. Liu and W. Cho Chew, *Appl. Phys. Lett.*, 2011, **99**, 113304.
96 M. Xue, L. Li, B. J. Tremolet de Villers, H. Shen, J. Zhu, Z. Yu, A. Z. Stieg, Q. Pei, B. J. Schwartz and K. L. Wang, *Appl. Phys. Lett.*, 2011, **98**, 253302.
97 D. H. Wang, D. Y. Kim, K. W. Choi, J. H. Seo, S. H. Im, J. H. Park, O. O. Park and A. J. Heeger, *Angew. Chem., Int. Ed.*, 2011, **50**, 5519–5523.
98 D. H. Wang, K. H. Park, J. H. Seo, J. Seifter, J. H. Jeon, J. K. Kim, J. H. Park, O. O. Park and A. J. Heeger, *Adv. Energy Mater.*, 2011, **1**, 766–770.
99 G. D. Spyropoulos, M. M. Stylianakis, E. Stratakis and E. Kymakis, *Appl. Phys. Lett.*, 2012, **100**, 213904.
100 I. Kim, T. S. Lee, D. S. Jeong, W. S. Lee, W. M. Kim and K.-S. Lee, *Opt. Express*, 2013, **21**, A669–A676.
101 G. Kakavelakis, E. Stratakis and E. Kymakis, *RSC Adv.*, 2013, **3**, 16288–16291.
102 G. Kakavelakis, E. Stratakis and E. Kymakis, *Chem. Commun.*, 2014, **50**, 5285–5287.
103 V. Kochergin, L. Neely, C.-Y. Jao and H. D. Robinson, *Appl. Phys. Lett.*, 2011, **98**, 133305.
104 J. Yang, J. You, C.-C. Chen, W.-C. Hsu, H.-R. Tan, X. W. Zhang, Z. Hong and Y. Yang, *ACS Nano*, 2011, **5**, 6210–6217.
105 L. Qiao, D. Wang, L. Zuo, Y. Ye, J. Qian, H. Chen and S. He, *Appl. Energy*, 2011, **88**, 848–852.
106 C. C. D. Wang, W. C. H. Choy, C. Duan, D. D. S. Fung, W. E. I. Sha, F.-X. Xie, F. Huang and Y. Cao, *J. Mater. Chem.*, 2012, **22**, 1206–1211.
107 D. H. Wang, J. K. Kim, G.-H. Lim, K. H. Park, O. O. Park, B. Lim and J. H. Park, *RSC Adv.*, 2012, **2**, 7268–7272.
108 N. Kalfagiannis, P. G. Karagiannidis, C. Pitsalidis, N. T. Panagiotopoulos, C. Gravalidis, S. Kassavetis, P. Patsalas and S. Logothetidis, *Sol. Energy Mater. Sol. Cells*, 2012, **104**, 165–174.
109 L. Li, Y. Zhang, S. Li, G. Li and W. Zhang, *Electrochim. Acta*, 2013, **87**, 277–282.
110 F. X. Xie, W. C. H. Choy, C. C. D. Wang, W. E. I. Sha and D. D. S. Fung, *Appl. Phys. Lett.*, 2011, **99**, 153304.
111 C.-M. Liu, C.-M. Chen, Y.-W. Su, S.-M. Wang and K.-H. Wei, *Org. Electron.*, 2013, **14**, 2476–2483.
112 B. Chen, W. Zhang, X. Zhou, X. Huang, X. Zhao, H. Wang, M. Liu, Y. Lu and S. Yang, *Nano Energy*, 2013, **2**, 906–915.
113 K. Jung, H.-J. Song, G. Lee, Y. Ko, K. Ahn, H. Choi, J. Y. Kim, K. Ha, J. Song, J.-K. Lee, C. Lee and M. Choi, *ACS Nano*, 2014, **8**, 2590–2601.
114 J. Grandidier, R. A. Weitekamp, M. G. Deceglie, D. M. Callahan, C. Battaglia, C. R. Bukowsky, C. Ballif, R. H. Grubbs and H. A. Atwater, *Phys. Status Solidi A*, 2013, **210**, 255–260.
115 R. B. Dunbar, H. C. Hesse, D. S. Lembke and L. Schmidt-Mende, *Phys. Rev. B: Condens. Matter Mater. Phys.*, 2012, **85**, 035301.
116 B. Wu, T. Z. Oo, X. Li, X. Liu, X. Wu, E. K. L. Yeow, H. J. Fan, N. Mathews and T. C. Sum, *J. Phys. Chem. C*, 2012, **116**, 14820–14825.
117 B. Wu, X. Liu, T. Oo, G. Xing, N. Mathews and T. Sum, *Plasmonics*, 2012, **7**, 677–684.
118 H. Gao, J. Henzie, M. H. Lee and T. W. Odom, *Proc. Natl. Acad. Sci. U. S. A.*, 2008, **105**, 20146–20151.
119 J. Zhu, M. Xue, H. Shen, Z. Wu, S. Kim, J.-J. Ho, A. Hassani-Afshar, B. Zeng and K. L. Wang, *Appl. Phys. Lett.*, 2011, **98**, 151110.
120 I. Kim, D. S. Jeong, T. S. Lee, W. S. Lee and K.-S. Lee, *Opt. Express*, 2012, **20**, A729–A739.
121 J. You, X. Li, F.-X. Xie, W. E. I. Sha, J. H. W. Kwong, G. Li, W. C. H. Choy and Y. Yang, *Adv. Energy Mater.*, 2012, **2**, 1203–1207.
122 M. A. Sefunc, A. K. Okyay and H. V. Demir, *Opt. Express*, 2011, **19**, 14200–14209.
123 M. Bora, E. M. Behymer, D. A. Dehlinger, J. A. Britten, C. C. Larson, A. S. P. Chang, K. Munechika, H. T. Nguyen and T. C. Bond, *Appl. Phys. Lett.*, 2013, **102**, 251105.
124 X. Li, W. C. H. Choy, L. Huo, F. Xie, W. E. I. Sha, B. Ding, X. Guo, Y. Li, J. Hou, J. You and Y. Yang, *Adv. Mater.*, 2012, **24**, 3046–3052.
125 S. H. Park, A. Roy, S. Beaupre, S. Cho, N. Coates, J. S. Moon, D. Moses, M. Leclerc, K. Lee and A. J. Heeger, *Nat Photon*, 2009, **3**, 297–302.
126 D. N. Congreve, J. Lee, N. J. Thompson, E. Hontz, S. R. Yost, P. D. Reusswig, M. E. Bahlke, S. Reineke, T. Van Voorhis and M. A. Baldo, *Science*, 2013, **340**, 334–337.

127 W.-F. Xu, C.-C. Chin, D.-W. Hung and P.-K. Wei, *Sol. Energy Mater. Sol. Cells*, 2013, **118**, 81–89.
128 Y. Jin, J. Feng, X.-L. Zhang, M. Xu, Y.-G. Bi, Q.-D. Chen, H.-Y. Wang and H.-B. Sun, *Appl. Phys. Lett.*, 2012, **101**, 163303.
129 W. Zhang, M. Saliba, S. D. Stranks, Y. Sun, X. Shi, U. Wiesner and H. J. Snaith, *Nano Lett.*, 2013, **13**, 4505–4510.
130 J. You, Z. Hong, Y. Yang, Q. Chen, M. Cai, T.-B. Song, C.-C. Chen, S. Lu, Y. Liu, H. Zhou and Y. Yang, *ACS Nano*, 2014, **8**, 1674–1680.